Available online at www.sciencedirect.com

SciVerse ScienceDirect

Acta Materialia 60 (2012) 4477–4486

Acta MATERIALIA

www.elsevier.com/locate/actamat

Structural response of A_2TiO_5 (A = La, Nd, Sm, Gd) to swift heavy ion irradiation

Cameron L. Tracy [a], Maik Lang [b], Jiaming Zhang [b], Fuxiang Zhang [b], Zhongwu Wang [c], Rodney C. Ewing [a,b,*]

[a] Department of Materials Science & Engineering, University of Michigan, Ann Arbor, MI 48109, USA
[b] Department of Earth and Environmental Sciences, University of Michigan, Ann Arbor, MI 48109, USA
[c] Cornell High Energy Synchrotron Source, Cornell University, Ithaca, NY 14853, USA

Received 18 March 2012; received in revised form 25 April 2012; accepted 3 May 2012
Available online 7 June 2012

Abstract

Different compositions of orthorhombic A_2TiO_5 (A = La, Nd, Sm, Gd) have been irradiated with swift Xe ions (1.47 GeV). Systematic analysis of the structural modifications induced by ion track formation was completed using transmission electron microscopy, synchrotron X-ray diffraction, and Raman spectroscopy. Significant radiation-induced amorphization occurred, but the size of the amorphous regions within the tracks decreased as smaller cations (higher Z) occupied the A-site. This decrease in the amorphous domain size is attributed primarily to epitaxial recrystallization of a disordered phase at the outer edge of the tracks, the stability of which is related to the ratio of the ionic radii of the A- and B-site (B = Ti) cations. While similar ion track recrystallization phenomena have been observed in pyrochlores of varying composition, A_2TiO_5 is unique in that the disordered phase is not a high-temperature polymorph, suggesting kinetic control of the radiation-induced transformation.

Keywords: Ion irradiation; Oxides; Phase transformations; Order–disorder phenomena

1. Introduction

Irradiation of insulators with swift heavy ions (having initial energies in the MeV to GeV range) causes a variety of structural modifications, including the formation of cylindrical damage zones, ion tracks, along the ion trajectory. Two mechanisms of track formation, the Coulomb explosion [1–3] and thermal spike models [3–5], have been proposed. Swift heavy ions interact primarily with the electrons of the irradiated material, but there are several mechanisms by which their energy is transferred to the solid. The Coulomb explosion model proposes that ionization of atoms in the ion path results in interatomic repulsion due to electrostatic forces, causing a radial pressure wave that destroys the long-range periodicity of the materials, leaving an ion track. Alternatively, the thermal spike model considers that the transfer of energy from electrons to atoms occurs by electron–phonon coupling, which leads to intense local heating of the material along the ion path. The thermal spike can induce phase transformations or, by rapid quenching due to the radial conduction of heat into the surrounding material, leave an amorphous core in the track [6].

While the specific processes by which tracks form are not fully established, ion tracks have been observed in a number of materials following irradiation with swift heavy ions above a critical value of ion energy loss (dE/dx), the value of which is material-dependent [7]. Within such tracks, both crystalline-to-amorphous [8] and crystalline-to-crystalline [9,10] phase transitions have been observed, along with tracks in which an amorphous core is surrounded by a disordered, but still crystalline, shell [11–13]. Materials that display the latter track morphology

* Corresponding author at: Department of Earth and Environmental Sciences, University of Michigan, Ann Arbor, MI 48109, USA.
E-mail address: rodewing@umich.edu (R.C. Ewing).

1359-6454/$36.00 © 2012 Acta Materialia Inc. Published by Elsevier Ltd. All rights reserved.
http://dx.doi.org/10.1016/j.actamat.2012.05.005

have generated a great deal of interest because these materials tend to disorder under irradiation rather than becoming amorphous and are promising candidates for applications in which radiation resistance is necessary [14]. Specifically, compounds within the A_2O_3–BO_2 binary (A = lanthanides, Y, and Sc; B = Ti, Zr, Sn, Hf) have been proposed as potential host materials for the immobilization of actinides and as inert matrix fuels for the transmutation of plutonium and the "minor" actinides (Np, Am, and Cm) in advanced fuel cycles [15–18]. Swift heavy ion irradiation provides a means of simulating the results of high-energy irradiation fields on a wide variety of materials. Furthermore, the relatively large damage zone volumes produced by this technique allows for characterization of the complex far-from-equilibrium behavior of materials.

The swift heavy ion irradiation response of many compounds within this system, including pyrochlore (of the general formula $A_2B_2O_7$) [11–13,19–22] and δ-phase ($A_4B_3O_{12}$) [23,24] materials, have been investigated. However, there exists only a single prior study of the behavior of compositionally related ordered A_2BO_5 phases [11]. A_2TiO_5 compounds find application in a variety of nuclear components. Dy_2TiO_5 is used as a neutron absorber in the control rods of Russian WWER-type reactors, where it offers significant swelling and He bubble formation improvements as compared with conventional boron steels and boron carbide [25,26]. Oxide-dispersion strengthened (ODS) ferritic alloys, developed in part to serve as radiation-damage-resistant structural materials for advanced reactors, contain nanoscale Y_2TiO_5 particles that provide superior mechanical properties in reactor environments [27,28]. In all of these applications the material is exposed to high radiation fluxes, making an understanding of this compound's phase behavior under such conditions crucial for its use.

At ambient pressure, A_2TiO_5 phases exhibit three polymorphs: orthorhombic, hexagonal, and isometric [29,30]. At room temperature the orthorhombic phase (*Pnam*) is stable when the A-site cations are larger than Er (La–Ho and Y). This structure, shown in Fig. 1a, consists of edge-sharing monocapped octahedra in which the A-site cation is coordinated with seven oxygen atoms, while Ti is five-coordinated with oxygen in a square pyramidal configuration that shares two edges (on the square planar portion) and a corner (at the pyramidal apex) with neighboring A-site polyhedra [31]. For compounds with A = Eu–Ho and Y, a high-temperature hexagonal polymorph ($P6_3/mmc$) with partial cation disordering is observed [32]. This structure exhibits a close-packed, six-layered ABABAB configuration along the 6_3 axis. A-site cations are octahedrally coordinated between the first and second and the fourth and fifth layers, in addition to partially occupying a mixed site on the third and sixth layer. Ti occupies the latter bipyramidal mixed site exclusively. In order to maintain charge balance, 20% of the mixed occupancy sites are vacant. Finally, compounds with small A-site cations (Er–Lu and Sc), crystallize in a defect

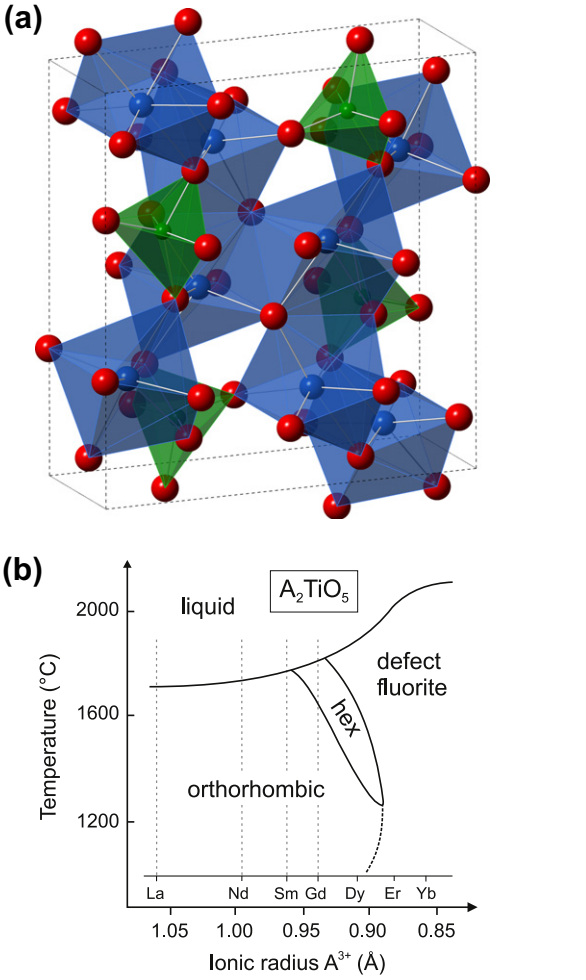

Fig. 1. (a) Schematic structure of orthorhombic A_2TiO_5 (*Pnam*). The square pyramidal polyhedra are TiO_5, where Ti is coordinated at an equal bond length with the four basal anions and at a slightly shorter bond length for the anion at the pyramidal apex. The edge-sharing monocapped octahedra are AO_7. (b) Thermal phase behavior of A_2TiO_5 compounds as a function of the A-site cation; adapted from Ref. [29].

fluorite phase (*Fm3m*) at ambient conditions. In this structure, both cation species occupy a single site in a non-ordered arrangement and charge compensation is achieved via vacancies on the anion sublattice. For A = Tb–Ho and Y, this cubic phase is stable at high temperatures, such that, upon heating, it will form after the hexagonal polymorph. This thermal phase behavior is illustrated in Fig. 1b, after Petrova et al. [29].

For those compositions that undergo a thermally driven transformation to a disordered phase (either the hexagonal or defect fluorite polymorphs), the temperature at which this order–disorder transformation occurs, $T_{O–D}$, is strongly dependent on the ionic radius of the A-site cation [29]. For example, Gd_2TiO_5 transforms to its hexagonal polymorph at ~1700 °C, while Dy_2TiO_5, having a smaller A-site cation, undergoes the same phase transformation at ~1350 °C. This trend of decreasing $T_{O–D}$ with the substitution of smaller cations can be explained in terms of the energetics of disordering of the material. Incorporation of

lanthanides or other large cations in the mixed occupancy sites of the disordered polymorphs gives rise to significant structural strain. Thus, those compositions for which the A-site cation is more similar in size to Ti will see a reduction in strain energy associated with the order–disorder transitions; therefore, an increase in the thermal stability of the disordered fluorite or hexagonal phases.

This thermally driven order–disorder transformation shows many similarities to those that occur in the pyrochlore structure upon heating, irradiation, and pressurization [33]. Under these conditions, many pyrochlores disorder on both their anion and cation sublattices, adopting a defect fluorite structure [19,34]. As observed for A_2TiO_5 materials, the temperature at which this transition occurs decreases with the substitution of smaller cations into the A-site. A correlation has been observed between the ratio of the ionic radii of the A- and B-site cations in the pyrochlore structure and the ratio of amorphous to disordered crystalline phase volumes within individual ion tracks of samples irradiated with swift heavy ions [12,13,19].

The only prior study of A_2TiO_5 materials investigated Gd_2TiO_5 irradiated with swift heavy ions, showing a similar track morphology to that seen in pyrochlores, with the amorphous track core surrounded by a ring of the high-temperature hexagonal phase [11]. This result suggests that the track formation processes in the two phases may be related and that chemical composition may be a critical parameter that governs the amount of radiation damage in both materials. For this reason, a detailed understanding of the compositional trends in the track size and morphology of irradiated A_2TiO_5 compounds is necessary in order to understand their radiation response and damage accumulation mechanisms. In this paper we present the first systematic study of swift heavy ion irradiation damage and ion track morphology in orthorhombic A_2TiO_5 compounds in which the A-site cation has been varied.

2. Experimental procedure

Powders of A_2TiO_5 (A = La, Nd, Sm, Gd) were synthesized by solid-state methods from well mixed A_2O_3 and TiO_2 powders. These powders were then compressed, using a hand press operating at low pressure, into flat sheets with a thickness of ~40 μm. After pressing, the samples were sintered for 24 h at 800 °C. Ion irradiation was completed using the X0 beamline of the UNILAC linear accelerator at the GSI Helmholtz Center for Heavy Ion Research in Darmstadt, Germany. All samples were simultaneously exposed to a beam of ^{132}Xe ions accelerated to 1.47 GeV. Calculations using the SRIM 2008 code [35], the results of which are shown in Fig. 2, projected ion ranges from 57 to 65 μm, indicating that all impinging ions passed completely through the samples. A relatively constant electronic energy loss, dE/dx, was achieved within the samples due to their thin size, such that uniformity of the ion tracks across the thickness of the samples can be assumed. The nuclear energy loss was projected to be several orders of magnitude lower than the electronic energy loss within the samples and was therefore neglected. Samples were irradiated at room temperature to several fluences in the range 5×10^{10}–1×10^{13} ions cm^{-2}, with typical fluence uncertainties of 10–20%. All samples of a given fluence were irradiated simultaneously and in the same sample holder in order to achieve consistent irradiation conditions.

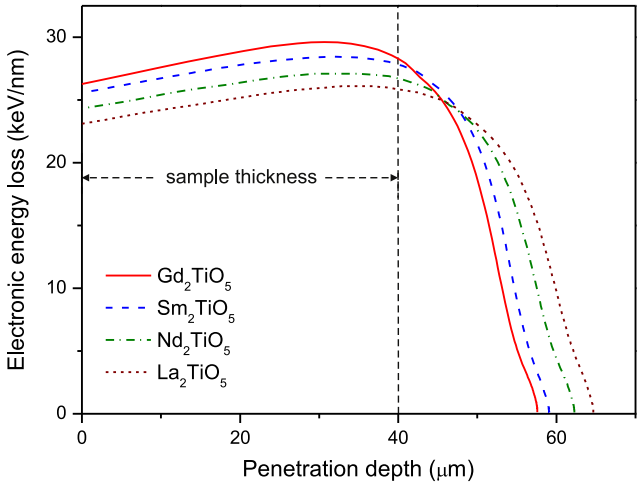

Fig. 2. Electronic energy loss as a function of penetration depth for all compositions tested, as calculated using SRIM 2008. The range of the 1.47 GeV ^{132}Xe ions is greater than the sample thickness for all materials and the energy loss within the sample thickness is relatively constant. The nuclear energy loss, which is not shown, is approximately three orders of magnitude less than the electronic energy loss within the sample thickness. Due to differences in density, the energy loss at a given penetration depth increases as the A-site is occupied by smaller cations.

After irradiation, the samples were characterized using angle-dispersive synchrotron X-ray diffraction (XRD) at the B2 beamline of the Cornell High Energy Synchrotron Source (CHESS). A monoenergetic beam ($\lambda = 0.496$) was operated in transmission mode with a spot size of 300 μm and the resulting diffraction rings were recorded with Mar charge coupled device (CCD) detectors. Integration of the plate images was performed using Fit2D software [36] and the resulting diffraction patterns were refined with Fullprof software [37]. The degree of irradiation-induced amorphization was quantitatively analyzed by deconvoluting these diffraction profiles in order to isolate diffraction intensity contributions from the crystalline and amorphous fractions, a process similar to that used in previous studies of pyrochlores [19]. Pseudo-Voigt functions were used in the peak fitting procedure. Semi-quantitative values of the total amorphous fraction were then obtained by taking the ratio of the integrated intensity of the broad amorphous peaks to that of the sharp crystalline peaks over the entire 2θ-range measured. Direct images of the ion tracks were obtained with a JEOL 2010F transmission electron microscope (TEM) operating at 200 kV. Samples were crushed into a fine powder after irradiation and deposited on a holey carbon TEM grid, such that tracks could be imaged in various orientations with respect to the electron beam. Track diameters were measured from bright field

images of a number of tracks from each composition. A JEOL 3011 TEM was used to analyze the atomic structure of individual tracks by means of high-resolution TEM. For this imaging, the pressed powder samples were thinned using a wedge polisher and ion mill to allow for imaging parallel to the ion track axis. Local structure modifications within the tracks were characterized with fast Fourier transform (FFT) analysis. Raman spectra were collected using a Renishaw inVia Raman Microscope with a 785 nm laser operating in backscattering geometry. A measuring time of 25 s was used for all samples and spectra were collected over a range of 100–1000 cm^{-1}. Multiple measurements were taken at different positions for each sample to test for orientation effects, which were not observed.

3. Results

3.1. Transmission electron microscopy

In order to image individual tracks without overlap, only samples irradiated to a fluence of 5×10^{10} ions cm^{-2} were analyzed by TEM. Representative images of tracks in La_2TiO_5, oriented approximately perpendicular to the electron beam, are shown in Fig. 3. The contrast between the tracks and the surrounding matrix is assumed to delineate the region that has undergone some ion-induced structural modification. The distance measured between the parallel track edges is considered to be the diameter of the ion tracks. However, because phase variation within the tracks cannot be distinguished and the different contributions of these track phases to the contrast observed is not quantified, the interpretation of these bright field images with respect to the morphology of these tracks is limited. Nevertheless, the measured diameters provide a clear indication of the extent to which different compositions sustain damage (including both crystalline-to-crystalline and crystalline-to-amorphous transitions) by swift heavy ions. The measured track diameters as a function of the ratio of the A- and B-site ionic radii are shown in Fig. 4 and summarized in Table 1. A linear trend is evident, with the track diameter, and therefore the volume of material damaged per ion, increasing as larger cations occupy the A-site.

HRTEM images were obtained with the axial track direction oriented parallel to the electron beam such that variation in the crystal structure of the ion tracks along the radial track direction could be observed. The use of swift heavy ions, which have enough energy to pass completely though the samples, allows for detailed analysis of radiation effects at the atomic scale by TEM because, when imaged in this orientation, only the damaged volume of the sample contributes to the track region in the resulting phase contrast image. Representative images for La_2TiO_5 (imaged on the [1 4 0] zone axis) and Sm_2TiO_5 (imaged on the [0 1 0] zone axis) are shown in Fig. 5. A small reduction in the diameter of the ion track, defined as the area in which some transformation from the orthorhombic matrix is observed, is evident and is consistent with the bright field images. However, significant differences in track morphology are seen for the two compositions. The sample containing La at the A-site features entirely amorphous tracks; no crystalline-to-crystalline transformation is evident within the track core or along its edge. In contrast, evidence of such a transformation is observed for the sample containing Sm. A large portion of this track, situated at its outer edge, shows a crystalline phase distinct from that of the orthorhombic matrix. FFT analysis confirmed a fluorite

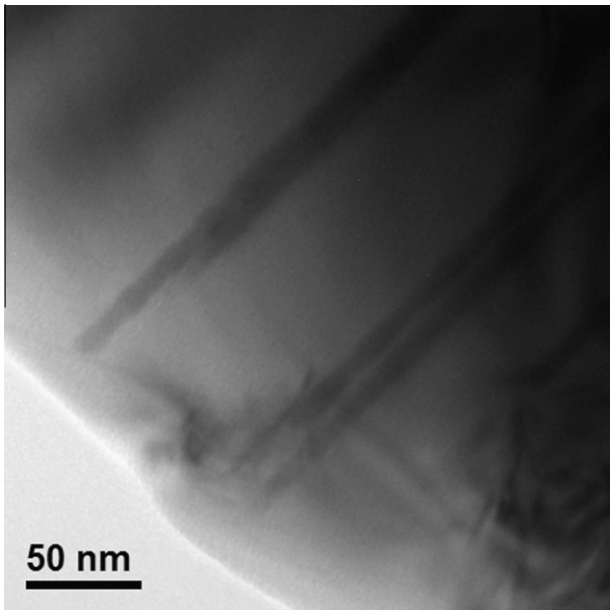

Fig. 3. Bright-field image of ion tracks in Ln_2TiO_5 irradiated with 1.47 GeV Xe ions to a fluence of 5×10^{10} ions cm^{-2}. The cylindrical tracks can be identified by contrast variation. Similar contrast was observed for all compositions examined.

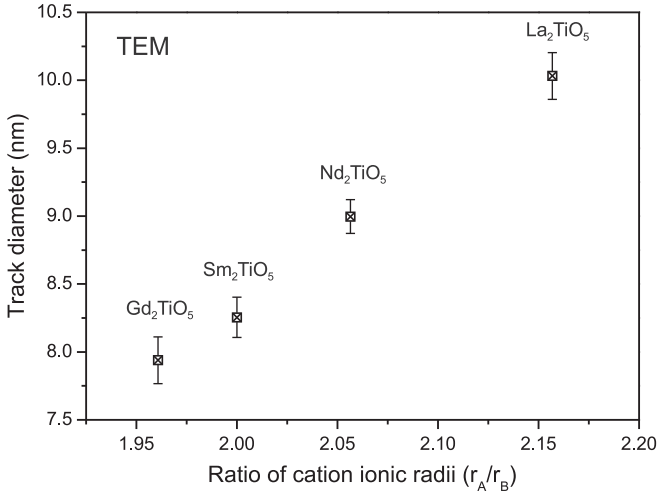

Fig. 4. Average track diameters, measured by bright-field TEM, as a function of the ratio of cation ionic radii in each compound investigated. A linear trend is evident. The error bars give the standard error of the mean for the measured tracks.

Table 1
Refined unit cell parameters, densities, and ion electronic energy losses for the compositions tested.

Composition	a (Å)	b (Å)	c (Å)	Density (g cm^{-3})	$(dE/dx)_e$ (keV nm^{-1})	Bright-field TEM d (nm)
La_2TiO_5	11.418(2)	11.035(4)	3.948(1)	5.417	24.6 ± 1.5	10.1 ± 0.2
Nd_2TiO_5	11.345(7)	10.743(5)	3.853(1)	5.889	25.7 ± 1.4	9.0 ± 0.1
Sm_2TiO_5	11.331(8)	10.607(2)	3.804(7)	6.226	27.0 ± 1.4	8.3 ± 0.1
Gd_2TiO_5	11.295(4)	10.496(2)	3.768(1)	6.578	27.9 ± 1.7	7.9 ± 0.2

Due to the increase in density for compounds incorporating the higher lanthanides, the ion energy transferred to the crystal per unit path length is largest for those compositions with smaller A-site cations. Track diameters were measured using bright-field TEM images.

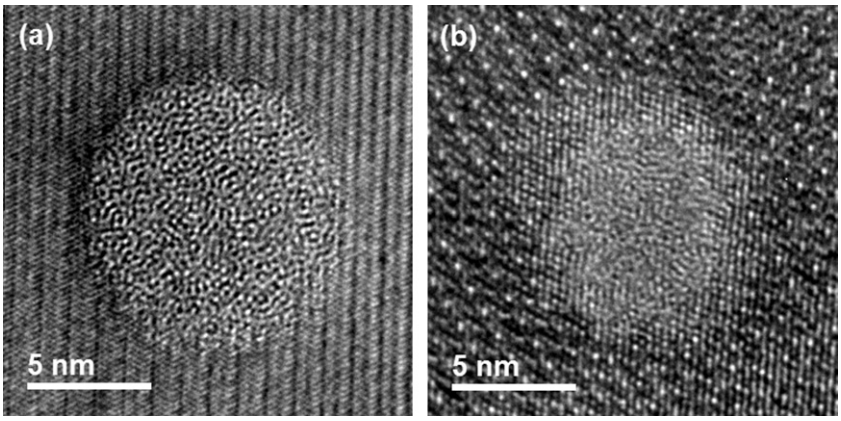

Fig. 5. (a) HRTEM image of an ion track in La_2TiO_5 along the [1 4 0] zone axis. This material shows the largest tracks of all compositions tested and exhibits only a single amorphous zone. The dark ring seen along the edge of the track is likely due to strain contrast. (b) HRTEM image of an ion track in Sm_2TiO_5 along the [0 1 0] zone axis. The central amorphous region is surrounded by a shell of a different structure than that of the orthorhombic matrix. FFT analysis confirms a defect fluorite shell. The total diameter of the track, including both fluorite and amorphous regions, is slightly smaller than that of La_2TiO_5, while the amorphous area is significantly reduced.

structure in this region, oriented along the [1 1 0] zone axis, rather than the high-temperature hexagonal polymorph which was previously reported in ion irradiated Gd_2TiO_5 [11].

Comparison of the HRTEM images with those taken perpendicular to the axial track direction reveals two distinct changes in track morphology with the reduction of the A-site cation size. When smaller cations occupy the A-site, the total track size (considering both disordered and amorphous regions) decreases and there is close agreement between both sets of TEM images in the magnitude of this decrease. This suggests that contrast in the bright field images arises from both the disordered and amorphous regions. The other effect of the smaller ions, which is only evident in the HRTEM images, is the presence of a disordered crystalline phase at the outer region of the tracks.

3.2. X-ray diffraction

Several diffraction patterns were obtained for samples irradiated to a range of fluences from 5×10^{10} ions cm^{-2} to 1×10^{13} ions cm^{-2}. The results of Rietveld refinement performed on the patterns taken from unirradiated samples are shown in Table 1. The unit cell parameters determined for all materials agree well with those reported in the literature [29,30,38–40]. Representative diffraction patterns, showing the evolution of the diffraction profiles with increasing radiation dose, are shown in Fig. 6. For all compositions the growth of three diffuse peaks, at 2θ ranges of ~7–12°, 12–20°, and 22–30°, is evident with increasing fluence due to scattering from amorphous regions within the ion track cores, confirming that, for all compositions, a crystalline-to-amorphous transformation is induced by swift heavy ion irradiation. The amorphous peaks observed are similar to those seen in swift heavy ion irradiated titanate pyrochlores for which amorphization occurred [12,19]. A corresponding decrease in the area of the sharp crystalline peaks with increasing fluence is present. Peaks corresponding to a fluorite structure were not observed, suggesting that the volume transformed is, for all fluences, too low to be detected by XRD.

Comparison of the profiles from different compositions shows, for a given fluence, a decrease in the ratio of the amorphous intensity to that of the crystalline fraction with the substitution of smaller cations on the A-site. This ratio of integrated intensities is treated as the fraction of amorphous phase in a sample. Note, however, that due to the complex relationship between peak intensities and the crystalline/amorphous phase distribution, the amorphous fractions presented should not be treated as absolute measurements of the volume of material amorphized by swift heavy ions [41]. Still, because the samples investigated exhibit the same primary structure and are of similar composition, the

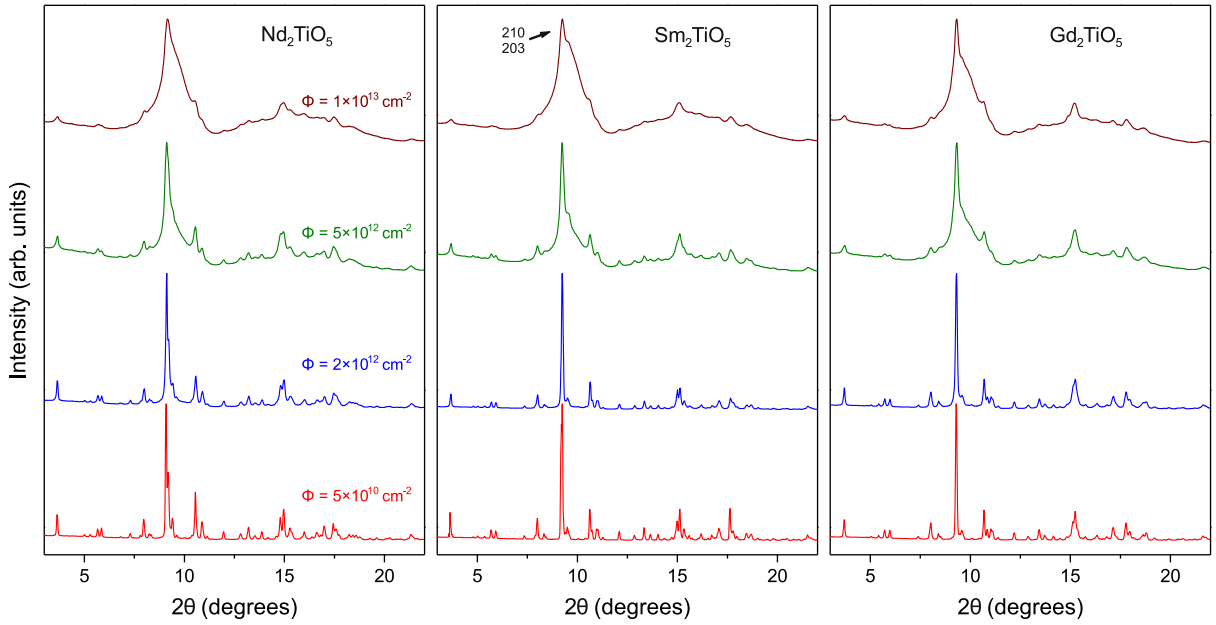

Fig. 6. Representative synchrotron XRD patterns ($\lambda = 0.496$) of three compositions for a range of ion irradiation fluences. Amorphization is evident as broad peaks due to diffuse scattering from the track core regions, while sharp peaks from crystalline domains, present at all fluences, indicate the presence of some degree of crystallinity. Increased crystallinity for the compositions with smaller A-site cations is most evident from the comparison of the (210) and (203) peaks, which overlap at high fluences.

dependence of the integrated intensities on the amorphous and crystalline phase proportions should be similar. Hence, these data illustrate the relative change in amorphization resistance of these materials that result from changes in the A-site cation. At the highest fluence achieved, 1×10^{13} ions cm^{-2}, the Nd_2TiO_5 composition is almost completely amorphized, with only small peaks from crystalline regions remaining. In contrast, the irradiated Gd_2TiO_5, while still displaying a significant reduction in the intensity of the peaks from crystalline areas and the presence of diffuse scattering, exhibits a greater degree of crystallinity and shows amorphous background peaks of lower intensity than in the samples with larger A-site cations.

The amorphous fractions determined for these materials using the deconvolution procedure described earlier exhibit an initial linear increase as a function of fluence, followed by a gradual reduction in the rate of amorphization as a function of fluence as the amorphization approaches saturation. The damage evolution is best described by a direct impact model of the form:

$$f_A(\Phi) = 1 - e^{-(\sigma\Phi)} \quad (1)$$

where f_A is the amorphous fraction for a given fluence, Φ, and σ is the cross-sectional area of the amorphous region produced by a single incident ion [42]. Fitting of this model to the data collected allowed for the determination of amorphous track core cross-sectional areas for each composition. A representative example of the amorphous fraction of Nd_2TiO_5 as a function of fluence as determined from the diffraction data, along with the corresponding fit to the direct impact model, Eq. (1), is shown in Fig. 7. The extracted amorphous cross-sectional area per incident ion is reported in Fig. 8 for all compositions, which is proportional to the ionic radii of the cations at the A-site. While track diameters can be calculated from these cross-sectional areas by assuming cylindrical track geometry, the qualitative nature of the method used to determine the amorphous fraction present in a given sample prevents

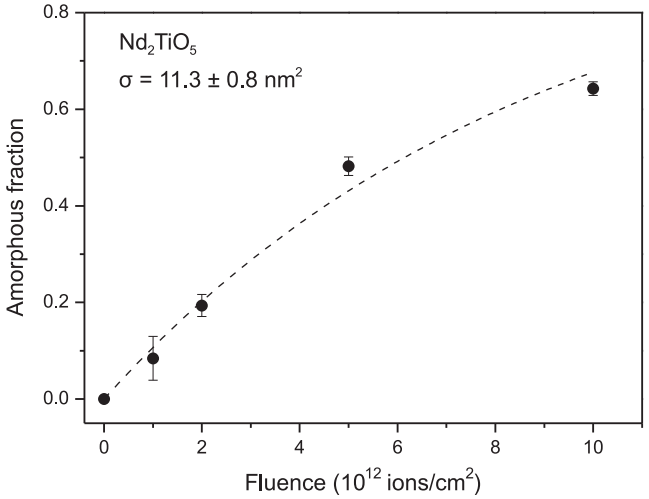

Fig. 7. Calculated amorphous fractions as a function of ion irradiation fluence for two compositions, along with results of the fitting of a direct impact model (Eq. (1)) to the data. Increased amorphization at a given fluence indicates an increase in the volume of material amorphized per ion. The deviation in the amorphous fraction determined for those samples irradiated at a measured fluence of 5×10^{12} ions cm^{-2} from the model is likely due to systematic fluence error in the experimental irradiation process. Error bars were derived from repeated deconvolutions of multiple synchrotron XRD patterns.

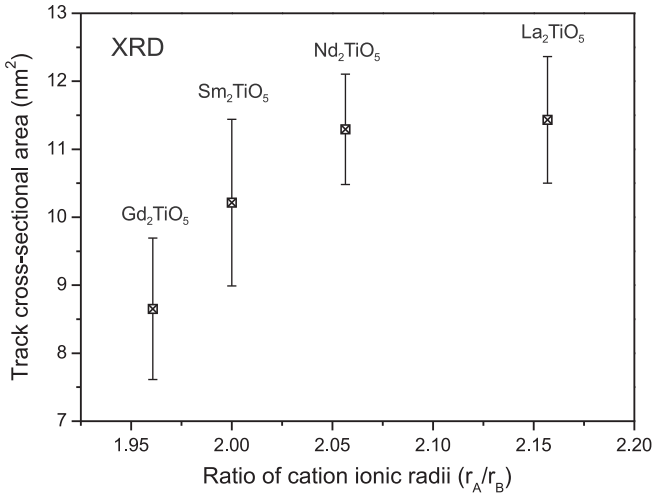

Fig. 8. Semi-quantitative track cross-sectional areas determined from the fitting of a direct impact model (Eq. (1)) to the XRD data as a function of the ratio of the ionic radius of the A-site cation to that of Ti. The error bars represent uncertainty in the fitting processes.

direct comparison of the track diameters determined using different characterization techniques. Nevertheless, these results support those obtained by TEM analysis (Fig. 4), as they show the same trend of decreasing degree of amorphization, which is attributed to both a reduction in overall track diameter and a reduction in the volume of the amorphous region of a partially crystalline track, with the reduction of the A-site cation size.

3.3. Raman spectroscopy

The Raman spectra are consistent with those obtained in previous studies of A_2TiO_5 materials [38,43]. As shown for Sm_2TiO_5 in Fig. 9, the large number Raman-active modes (48 are predicted by vibrational analysis) result in a complex spectrum. Raman modes were assigned to the peaks following Paques-Ledent [43], with the bands above 350 cm^{-1} attributed to internal vibrations of the TiO_5 polyhedra, while those below are attributed to translational modes of the A-site cation and, for the intense peaks at ~167 and 335 cm^{-1}, both the A-site and Ti cations.

As with the XRD results, two modifications to the Raman spectra were observed following irradiation. The sharp peaks present in the unirradiated materials broadened and decreased in intensity, with both changes increasing in magnitude with increasing fluence. Because the peaks can be distinguished by way of the polyhedra that contribute to their intensity, the reduction in the intensities of the crystalline peaks were compared, with representative results reported in Fig. 10 for a fluence of 2×10^{12} ions cm^{-2}, for which the background contribution from the amorphous phase is minimal. A large range of intensity reductions was observed for the different Raman modes, with no clear dependence of the reduction on the polyhedra involved. A similar lack of dependence of the vibrational mode intensity reduction on the contributing polyhedra was seen for all

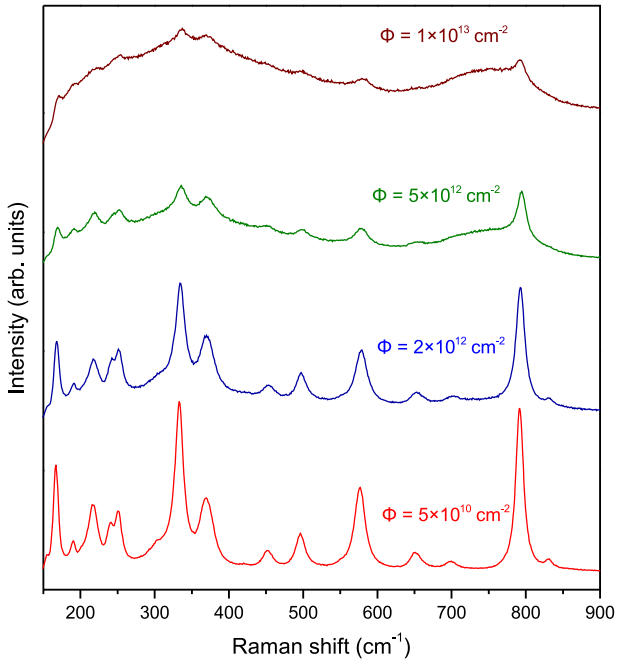

Fig. 9. Raman spectra of Sm_2TiO_5 for four ion fluences. The virgin sample shows bands representative of the orthorhombic A_2TiO_5 structure, all of which decrease in intensity as the ion fluence increases. Additionally, a broad background signal increases in intensity at higher fluences, with an identifiable band at ~740 cm^{-1}.

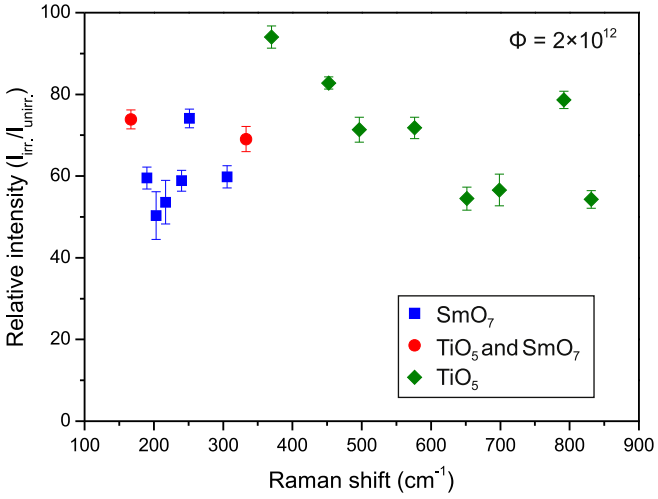

Fig. 10. Reduction of intensity of the Sm_2TiO_5 Raman peaks with ion irradiation, presented here as the intensity of individual peaks from the spectrum of a sample irradiated to a fluence of 2×10^{12} ions cm^{-2} relative to those of an unirradiated sample. Identification of the polyhedral from which each band originates does not show a clear trend, suggesting a uniform effect of ion irradiation on the structure.

fluences. The second modification to the Raman spectra that is evident with ion irradiation is the growth of a large asymmetric background signal. Of particular interest is the Gaussian band centered at ~740 cm^{-1}, which is similar to that formed for titanate pyrochlores irradiated with swift heavy ions [12]. Even at the highest fluence there was no band that could be assigned to the fluorite structure, even

though it is clearly present in the shell of the tracks of compositions with small A-site cations. However, the random distribution of O atoms in the disordered defect fluorite phase yields only a single, broad Raman band that is probably indistinguishable from the irradiation-induced background signal at the low fluorite volumes present in the irradiated samples.

4. Discussion

All compositions investigated show significant amorphization with irradiation, evidenced by the diffuse background signals in both XRD and Raman results and the lack of periodicity in the central regions of tracks imaged by TEM. In particular, the Raman results, which show no evidence of differential intensity reduction with respect to the polyhedra from which active bands originate, suggest that amorphization proceeds as a uniform transformation of the periodic atomic structure into the aperiodic state. The diffuse, high frequency band that increases in intensity with increasing fluence at $\sim$740 cm^{-1} may indicate, however, that Ti coordination shows little or no change with amorphization, as Sanjuán et al. have attributed a similar band in highly damaged pyrochlore titanates to Ti in either 5 or 5 + 1 coordination on the basis of spectroscopic analysis [44]. This band is positioned at a slightly lower frequency than that of the sharp crystalline band at $\sim$790 cm^{-1}, which corresponds to the short Ti–O bond between the Ti and the O at the apex of the TiO_5 pyramid. This agrees with the conclusion of Sanjuán et al. as, if it is assumed that the TiO_5 coordination is preserved but the structure of the square pyramidal polyhedra is distorted within the amorphous phase, the broad band at $\sim$740 cm^{-1} can be attributed to a vibrational mode of the Ti–O bond in this distorted coordination complex. In this modified coordination, the loss of long range periodicity in the A_2TiO_5 structure should result in some degree of averaging of the polyhedron's Ti–O bond lengths in comparison to the undamaged structure. Therefore, a reduction in the mean bond length of the TiO_5 complex bonds that contribute to the Raman spectrum is expected, causing a small decrease in the Raman shift of this broad peak with respect to that at $\sim$790 cm^{-1}. Regardless, the absence of long-range order in the track core results from the extensive damage introduced by the impinging ions.

Both TEM (Fig. 4) and XRD (Fig. 8) characterization of these materials show proportionality between the ionic radius of the A-site cation and the overall track diameter, as well as the ratio of amorphous-to-crystalline area within individual tracks. The actual changes are probably of a greater magnitude than indicated by these data, as the ion energy loss (Table 1) is greater for those compositions having smaller A-site cations. Such an increase in energy deposition would be expected to introduce more damage to a larger volume of the material. Therefore a significant increase in swift heavy ion radiation tolerance, or the ability to maintain crystallinity in such an environment, is seen for the compositions with a lower r_A/r_B ratio. This effect is comparable to that found in related pyrochlore compositions [19], in which it is attributed to the stability of the defect fluorite structure that recrystallizes from the melt region of ion tracks [11].

Because the disordered defect fluorite structure is observed as a track shell of Sm_2TiO_5, the increased post-irradiation crystallinity of those containing smaller lanthanides can be, in part, attributed to a similar recrystallization effect. However, the melting temperature of these titanates as one moves across the lanthanide series follows a similar trend (Fig. 1b), increasing by $\sim$50 °C between La_2TiO_5 and Gd_2TiO_5, such that it likely affects the track size as well [29]. According to the thermal spike model, an increase in the melting temperature, T_m, should result in smaller damaged regions, including both regions that have undergone a crystalline-to-amorphous transition and those that have undergone a transition to a second crystalline phase, but there should be no effect on the ratio of the cross-sectional areas of the two regions. We have shown exactly this result, as the overall track diameter imaged in bright field TEM (Fig. 4) decreases for the smaller lanthanides in the A-site. However, this reduction in track size is small as compared with the reduction in the diameter of the amorphous track core (Fig. 5), indicating that the majority of the resistance to amorphization accompanying the smaller A-site cations is due to the crystalline-to-crystalline transformation that occurs along the outer shell of the ion tracks. Compositional effects on the radiation response of these compounds are therefore attributed primarily to the stability of the disordered phases that form during the track-formation process. While clearly related to the disordering that occurs in pyrochlore titanates under similar irradiation conditions, the transition in these materials differs in that it involves a complete reconstruction of the crystal to a nonequilibrium phase (orthorhombic to defect fluorite, with the possibility of an intermediate liquid-like state from which recrystallization can occur), rather than simply the introduction of antisite defects on the cation sublattice and disordering of vacancies and O atoms on its anion sublattice.

Similar oxide crystalline-to-crystalline transformations following swift heavy ion irradiation have been observed in zirconia and hafnia, both of which transform from monoclinic to tetragonal phases [10]. Still, the radiation response of these materials is distinct from that of A_2TiO_5 in that their irradiation-induced phase is a high-temperature polymorph of both compounds. The transformation can therefore be described using a simple thermal spike model with the monoclinic-tetragonal transition temperature substituted for T_m [45]. In contrast, the A_2TiO_5 transformation yields a nonequilibrium phase, the formation of which cannot be accounted for thermodynamically. A thermally driven transformation directly from the orthorhombic phase to fluorite is unlikely, suggesting instead a kinetically controlled recrystallization of the latter phase, as predicted by molecular dynamics simulations of swift heavy ion irradiated pyrochlore titanates that are based

on the thermal spike model [11]. In the proposed track-formation process, quenching of the thermal spike occurs on a timescale that allows for some extent of recrystallization to occur, given suitably rapid kinetics. Because the formation of a fully ordered orthorhombic structure from an amorphous melt proceeds too slowly to allow for recovery of this phase prior to quenching of the track by the surrounding material, only structures that easily incorporate disorder, such as defect fluorite and, to a lesser extent, the hexagonal polymorph of A_2TiO_5, are able to form. An epitaxial relationship between the disordered phase and the surrounding matrix explains the track shell morphology, as the interface between the two phases serves as a nucleation site for crystallization.

Such a track-formation process supports the use of a direct impact model to describe damage accumulation in these materials, as is assumes that most or all of the track region adopts a liquid-like state immediately following energy transfer from the ion. Thus, the track-formation process should be insensitive to the initial structure of the region, which would exclude the use of a multiple impact model in which ion-induced phase evolution occurs by incremental structural modifications over the course of several ion impacts. However, the correct damage accumulation model for these materials cannot be definitively determined without the use of highly accurate data from low-fluence irradiations, for which significant differences in the amorphous fractions predicted by direct and multiple impact models exist [13].

By adopting this description of ion track formation in A_2TiO_5 materials, the effects of composition on ion track morphology can be accounted for by considering the energetics of the crystallization of fluorite from the melt. The ideal fluorite structure is most closely approximated for those compositions with a small r_A/r_B value, hence the stability of the phase in these compounds should increase as one moves across the lanthanide series. The reduction in energy that accompanies the amorphous-to-defect fluorite transformation serves as the driving force for crystallization, leading to the observed increase in resistance to irradiation-induced amorphization for those compositions with smaller A-site cations. In this way, the compositional effects on the radiation response of these materials to swift heavy ions are attributed to the role of the crystallization of a disordered phase from the melted thermal spike region, analogous to the crystallization phenomenon identified in pyrochlores. Interestingly, the same relationship between the extent to which amorphization is limited by the formation of defect fluorite and the ratio r_A/r_B in pyrochlores exists for the compositions investigated here. Calorimetry of A_2TiO_5 (A = La, Nd, Gd) shows a reduction in formation enthalpy with an increase in the ratio of the cation ionic radii [46]. This suggests that increased stability of the orthorhombic phase inhibits the recovery of a disordered phase, resulting in less recrystallization of the amorphized volume. The lack of a disordered shell in La_2TiO_5 further indicates that, for a certain ion energy loss, some critical cation radius ratio exists, above which recrystallization will not occur due to insufficient stability of the disordered phase.

The formation of a disordered defect fluorite structure in the track shell of Sm_2TiO_5 is of particular interest, as previous work on swift heavy ion irradiated Gd_2TiO_5 showed the formation of the hexagonal polymorph in this region [11]. HRTEM images of this composition could not be obtained for these samples, so a direct comparison cannot be made. However, this discrepancy may be explained by the phase energetics of the A_2TiO_5 system, as the hexagonal phase is stable only for compositions with an A-site cation smaller than Sm. Additionally, the previous study [11] used 2.2 GeV Au ions, which have a higher energy loss than those used for this work and might therefore exhibit different track-formation processes.

5. Conclusion

Swift heavy ion irradiation of A_2TiO_5 (A = La, Nd, Sm, Gd) compounds induces both crystalline-to-amorphous and crystalline-to-crystalline phase transformations within single ion tracks, for which the extent of the transformation depends on the size of the A-site cation. For those compositions for which both transformations occur, a shell morphology is observed in which the amorphous ion track core is surrounded by a concentric ring of disordered defect fluorite material. The ratio of crystalline-to-amorphous volume within a track increases as the ionic radius of the A-site cation decreases, suggesting increased stability of the disordered phase. The formation of this metastable disordered structure depends on the kinetics of the crystallization of the disordered phase from the melted region near the center of the ion-induced thermal spike. Quenching of the outer region of the track occurs on such a rapid time scale that complete ordering of the cations to the orthorhombic structure of the surrounding undamaged matrix cannot be achieved, resulting in the formation of a disordered phase. This model of track formation in A_2TiO_5 is closely related to the track formation process in pyrochlores, $A_2B_2O_7$, of similar composition and is consistent with the results of molecular dynamics calculations based on the thermal spike model.

Acknowledgements

This work was supported by the Materials Science of Actinides Center, and Energy Frontier Research Center funded by the US Department of Energy, Office of Science, Office of Basic Energy Sciences under Award Number DE-SC0001089. CLT acknowledges a Rackham Fellowship from the University of Michigan. The authors gratefully acknowledge technical support during the irradiation by the Materials Research Group at GSI. This work is based upon data collected at the Cornell High Energy Synchrotron Source (CHESS), which is supported by the National Science Foundation and the National Institutes of Health/

National Institute of General Medical Sciences under NSF Award DMR-0936384. TEM instrumentation at the Electron Microbeam Analysis Laboratory at the University of Michigan is supported by NSF Grants DMR-9871177 and DMR-0723032.

References

[1] Bullough R. J Appl Phys 1966;37:2283.
[2] Fleischer RL. J Mater Sci 2004;39:3901.
[3] Bringa E, Johnson R. Phys Rev Lett 2002;88:1.
[4] Toulemonde M. Nucl Instrum Methods Phys Res Sect B 2000;166–167:903.
[5] Szenes G. Nucl Instrum Methods Phys Res Sect B 1996;116:141.
[6] Schiwietz G, Czerski K, Roth M, Staufenbiel F, Grande P. Nucl Instrum Methods Phys Res Sect B 2004;225:4.
[7] Liu J, Neumann R, Trautmann C, Müller C. Phys Rev B 2001;64:184115.
[8] Meftah A, Brisard F, Costantini J, Dooryhee E, Hage-Ali M, Hervieu M, et al. Phys Rev B 1994;49:12457.
[9] Benyagoub A, Levesque F, Couvreur F, Gibert-Mougel C, Dufour C, Paumier E. Appl Phys Lett 2000;77:3197.
[10] Benyagoub A. Phys Rev B 2005;72:094114.
[11] Zhang J, Lang M, Ewing RC, Devanathan R, Weber WJ, Toulemonde M. J Mater Res 2011;25:1344.
[12] Lang M, Lian J, Zhang J, Zhang FX, Weber W, Trautmann C, et al. Phys Rev B 2009;79:224105.
[13] Sattonnay G, Grygiel C, Monnet I, Legros C, Herbst-Ghysel M, Thomé L. Acta Mater 2012;60:22.
[14] Sickafus KE, Minervini L, Grimes R, Valdez J, Ishimaru M, Li F, et al. Science 2000;289:748.
[15] Weber WJ, Rubia T. J Mater Res 1998;13:1434.
[16] Lutique S. J Nucl Mater 2003;319:59.
[17] Wang SX, Begg B, Wang LM, Ewing R, Weber W, Kutty K. J Mater Res 1999;14:4470.
[18] Ewing RC, Weber WJ, Lian J. J Appl Phys 2004;95:5949.
[19] Lang M, Zhang FX, Ewing RC, Lian J, Trautmann C, Wang Z. J Mater Res 2009;24:1322.
[20] Zhang J, Lang M, Lian J, Liu J, Trautmann C, Della-Negra S, et al. J Appl Phys 2009;105:113510.
[21] Jozwik-Biala I, Jagielski J, Thomé L, Arey B, Kovarik L, Sattonnay G, et al. Nucl Instrum Methods Phys Res Sect B, in press.
[22] Sattonnay G, Thomé L, Monnet I, Grygiel C, Legros C. Nucl Instrum Methods Phys Res Sect B, in press.
[23] Tang M, Kluth P, Zhang J, Patel MK, Uberuaga BP, Olson Reichhardt CJ, et al. Nucl Instrum Methods Phys Res Sect B 2010;268:3243.
[24] Tang M, Wynn T, Patel MK, Won J, Monnet I, Pivin JC, et al. J Nuc Mater 2012;425:193.
[25] Risovany VD, Varlashova EE, Suslov DN. J Nucl Mater 2000;281:84.
[26] Sinha A, Sharma BP. J Am Ceram Soc 2005;88:1064.
[27] Jiang Y, Smith JR, Odette G. Acta Mater 2010;58:1536.
[28] Yamashita S, Ohtsuka S, Akasaka N, Ukai S, Ohnuki S. Philos Mag Lett 2004;84:525.
[29] Petrova MA, Grebenshchikov RG. Glass Phys Chem 2008;34:603.
[30] Shepelev YF, Petrova MA. Inorg Mater 2008;44:1354.
[31] Mumme WG, Wadsley AD. Acta Crystallogr B 1968;24:1327.
[32] Shepelev YF, Petrova MA, Novikova AS. Glass Phys Chem 2004;30:342.
[33] Zhang FX, Wang J, Lian J, Lang M, Becker U, Ewing RC. Phys Rev Lett 2008;100:045503.
[34] Shlyakhtina AV, Shcherbakova LG. Solid State Ionics 2011;192:200.
[35] Ziegler JF, Ziegler MD, Biersack JP. Nucl Instrum Methods Phys Res Sect B 2010;268:1818.
[36] Hammersley AP. FIT2D, ESRF, Grenoble, France; 1998.
[37] Rodriguez-Carvajal J. FULLPROF2K, France; 2001.
[38] Zhang FX, Wang JW, Lang M, Zhang JM, Ewing RC. J Solid State Chem 2010;183:2636–43.
[39] Niu H, Gou H, Ewing RC, Lian J. MRS Proc 2011;1298:7.
[40] Preuss A, Gruehn R. J Solid State Chem 1994;110:363.
[41] Weber W, Hess N, Maupin G. Nucl Instrum Methods Phys Res Sect B 1992;65:102.
[42] Weber W. Nucl Instrum Methods Phys Res Sect B 2000;166–167:98.
[43] Paques-Ledent MT. Spectrochim Acta Part B 1976;32:1339.
[44] Sanjuán M, Guglieri C, Díaz-Moreno S, Aquilanti G, Fuentes A, Olivi L, et al. Phys Rev B 2011;84:104207.
[45] Benyagoub A. Nucl Instrum Methods Phys Res Sect B 2006;245:225.
[46] Hayun S, Navrotsky A. J Solid State Chem 2012;187:70.